J. Fluid Mech. (2022), *vol*. 952, R5, doi:10.1017/jfm.2022.946

Swimming in potential flow

Alec Glisman[1] **and John F. Brady**[1],†

[1]Division of Chemistry and Chemical Engineering, California Institute of Technology, Pasadena, CA 91125, USA

(Received 28 August 2022; revised 5 October 2022; accepted 7 November 2022)

The well-known self-propulsion, or swimming, of a deformable body in Stokes flow (i.e. at low Reynolds number) can be understood and modelled from the variation in the configuration-dependent hydrodynamic resistance tensor throughout the period of deformation. Remarkably, at the other extreme of high Reynolds number, a deformable body may also self-propel without doing any net work on the fluid in potential flow. As a body deforms, the mass of fluid displaced – the so-called added mass – depends on the instantaneous body configuration, and a net displacement is possible over a period of deformation. This potential swimming takes a form identical to that for Stokes swimmers with the configuration-dependent added mass replacing the hydrodynamic resistance tensor. Analytical insight into the swimming of a deformable body is obtained through an expansion of the nonlinear spatial dependence of the hydrodynamic interactions and connections between previous studies of swimming in Stokes flow to those in potential flow are made.

Key words: propulsion, active matter

1. Introduction

Self-propulsion is a vital element for life, from microscopic bacteria to large mammals. Swimming and flying organisms often deform their bodies to propel via hydrodynamic interactions with the surrounding fluid (Saffman 1967; Lighthill 1975; Najafi & Golestanian 2004; Swan *et al.* 2011). The essential fluid mechanics of propulsion varies between microscopic and macroscopic regimes as measured by the Reynolds number, $Re = \rho_f UL/\mu$, which quantifies the relative importance of inertial to viscous forces. The mass density ρ_f and viscosity μ of the fluid are material parameters, while the body's size and average swim speed set the characteristic length L and velocity U scales, respectively. Microorganisms self-propel at low Reynolds numbers, while larger bodies, such as birds and fish, self-propel at high Reynolds numbers (Klotsa 2019).

† Email address for correspondence: jfbrady@caltech.edu

The simplest model of fluid motion at large Reynolds numbers is potential flow, which approximates the flow field as irrotational and incompressible (Lamb 1924). Irrotational flow cannot model the process of vortex shedding as a means of self-propulsion, which has often been considered an essential element (Lighthill 1975; Wu, Brokaw & Brennen 1975).

This raises the question: Can a body self-propel in potential flow? The answer is yes, as first demonstrated by Saffman (1967) (see also Wu 1971; Kanso *et al.* 2005). The result is especially interesting, as the net motion occurs without dissipation and without the body doing net work on the fluid. Saffman argued that by breaking the natural time-reversal symmetry inherent in an irrotational flow, propulsion was generated from the configuration-dependent hydrodynamic (pressure) forces. Chambrion, Giraldi & Munnier (2019) revealed a more general requirement of self-propulsion based on geometric arguments of the system phase space showing that the same principle holds in both flow regimes.

In this paper we explore the connection between these two regimes by presenting the equations of motion governing swimming in both Stokes and potential flow. The equations of motion for self-propulsion are derived for a general particle-based swimmer and then analysed for a simple swimmer design called the collinear swimmer. We then 'race' the swimmer in both flow regimes for small and large amplitude body deformations. It is analytically predicted – and numerically confirmed – that for the given swimmer design, the Stokes swimmer translates farther due to its longer-ranged leading-order hydrodynamic interactions. The analytical predictions for net translation at small oscillation are found to remain accurate even as the oscillation becomes large. We conclude with a physically motivated discussion on how the results might be further generalized to study dissipative potential flows as well as understanding the role of hydrodynamic interactions in many swimmer systems.

2. Theory

To demonstrate the similarities between potential and Stokes flow, we first review the well-known theory and expressions for self-propulsion in Stokes flow (Stone & Samuel 1996; Lauga & Powers 2009; Swan *et al.* 2011; Masoud & Stone 2019). For convenience, we model the deformable body as a collection of N spherical particles connected together via non-hydrodynamic interparticle forces, e.g. springs, as illustrated in figure 1. The force balance on particle α is

$$0 = -\sum_{\beta=1}^{N} \boldsymbol{R}_{\alpha\beta} \cdot \boldsymbol{U}_\beta + \boldsymbol{F}^C_\alpha, \tag{2.1}$$

where $\boldsymbol{U}_\beta$ is the translational velocity of particle β, $\boldsymbol{R}_{\alpha\beta}(\{\boldsymbol{X}\})$ is the configuration-dependent hydrodynamic resistance tensor that couples force to velocity and $\boldsymbol{F}^C_\alpha$ is the interparticle connector force. Here, $\{\boldsymbol{X}\} = (\boldsymbol{x}_1, \ldots, \boldsymbol{x}_N)$ denotes the configuration of all N particles. To most clearly illustrate the behaviour, we consider only translational motion and forces; the necessary extensions to rotary motion and torques are discussed in Appendix A.

Self-propulsion is a force-free motion: there is no external force and the sum over all particles of the internal connector forces is zero, $\sum_\alpha \boldsymbol{F}^C_\alpha = 0$, thus

$$0 = -\sum_{\alpha,\beta=1}^{N} \boldsymbol{R}_{\alpha\beta} \cdot \boldsymbol{U}_\beta. \tag{2.2}$$

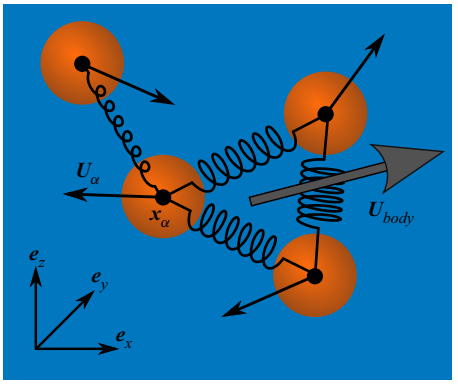

Figure 1. N spherical particles connected together to form a deformable body. Each particle α is parametrized by its position $\boldsymbol{x}_\alpha$ and velocity $\boldsymbol{U}_\alpha$. In general, the particle motion results in a net body velocity $\boldsymbol{U}_{body}$.

Selection of the spatial origin is arbitrary, and so we choose particle 1 for convenience as the body locator point and refer all motion relative to it. Alternatively, one could use the centre of mass or centre of resistance. We define a new set of relative coordinates and translational velocities,

$$\boldsymbol{r}_\alpha = \boldsymbol{x}_\alpha - \boldsymbol{x}_1, \quad \boldsymbol{V}_\alpha = \boldsymbol{U}_\alpha - \boldsymbol{U}_1, \tag{2.3a,b}$$

and the total force balance becomes

$$0 = -\boldsymbol{R}_{body} \cdot \boldsymbol{U}_1 - \sum_{\alpha,\beta=1}^{N} \boldsymbol{R}_{\alpha\beta} \cdot \boldsymbol{V}_\beta, \tag{2.4}$$

where the resistance tensor of the entire body is $\boldsymbol{R}_{body} = \sum_{\alpha,\beta=1}^{N} \boldsymbol{R}_{\alpha\beta}$. The translation of the body follows as

$$\boldsymbol{U}_1 = -\boldsymbol{R}_{body}^{-1} \cdot \sum_{\alpha,\beta=1}^{N} \boldsymbol{R}_{\alpha\beta} \cdot \boldsymbol{V}_\beta. \tag{2.5}$$

Since the absolute position in space for an isolated body does not matter, the resistance tensors are functions of the relative coordinates $\{\boldsymbol{r}_\alpha\}$ only.

We are interested in sustained motion of the body as it executes periodic deformation with period T. The net displacement of the body in one period is

$$\Delta\boldsymbol{x}_1 = -\int_0^T \boldsymbol{R}_{body}^{-1}(t) \cdot \sum_{\alpha,\beta=1}^{N} \boldsymbol{R}_{\alpha\beta}(t) \cdot \boldsymbol{V}_\beta(t)\, \mathrm{d}t, \tag{2.6}$$

where we emphasize that both the relative velocities $\boldsymbol{V}_\beta(t)$ and the resistance tensors are functions of time, the latter through the changing configuration $\{\boldsymbol{r}_\alpha(t)\}$. Since the articulation velocities $\boldsymbol{V}_\beta(t)$ are periodic in time, there will only be net displacement if the body configuration resistance tensors also change in time. This can be made more transparent by noting that $\boldsymbol{V}_\beta = \mathrm{d}\boldsymbol{r}_\beta/\mathrm{d}t = \dot{\boldsymbol{r}}_\beta$ and integrating (2.6) by parts:

$$\Delta\boldsymbol{x}_1 = \int_0^T \sum_{\alpha,\beta,\gamma} \nabla_{\boldsymbol{r}_\gamma} \cdot \left(\boldsymbol{R}_{body}^{-1} \cdot \boldsymbol{R}_{\alpha\beta}\right) : \boldsymbol{r}_\beta \dot{\boldsymbol{r}}_\gamma \, \mathrm{d}t, \tag{2.7}$$

showing that it is necessary for the resistance tensors to change with the internal configuration of the body to achieve net motion.

Turning now to potential flow, the absence of vorticity allows the fluid velocity $\boldsymbol{u}$ to be determined from the velocity potential $\boldsymbol{u} = \nabla\phi$, which satisfies Laplace's equation $\nabla^2\phi = 0$ subject to no flux conditions on the particle surfaces $\boldsymbol{n}\cdot\nabla\phi = \boldsymbol{n}\cdot\boldsymbol{U}_\alpha$, where $\boldsymbol{n}$ is the normal to the particle surface pointing into the fluid. The kinetic energy of the fluid $\mathcal{T}_f = \frac{1}{2}\rho_f\int \boldsymbol{u}\cdot\boldsymbol{u}\,\mathrm{d}V$ can be written in terms of the velocity potential and use of the divergence theorem gives

$$\mathcal{T}_f = \frac{1}{2}\sum_{\alpha,\beta}\boldsymbol{U}_\alpha\cdot\boldsymbol{M}_{\alpha\beta}(\{\boldsymbol{X}\})\cdot\boldsymbol{U}_\beta, \tag{2.8}$$

where the configuration-dependent $\boldsymbol{M}_{\alpha\beta}$ is known as the added mass. For example, the added mass of an isolated spherical particle is $\frac{1}{2}\rho_f V_p$, where V_p is the volume of the particle, and expresses the fact that a certain amount of fluid must be set into motion as the particle accelerates (Lamb 1924). How much fluid needs to be accelerated depends on the relative configuration of all N particles. To obtain the total kinetic energy $\mathcal{T}$ of the system, we add the kinetic energy of the individual particles $\frac{1}{2}m_\alpha U_\alpha^2$ to that of the fluid:

$$\mathcal{T} = \frac{1}{2}\sum_{\alpha,\beta}\boldsymbol{U}_\alpha\cdot\tilde{\boldsymbol{M}}_{\alpha\beta}(\{\boldsymbol{X}\})\cdot\boldsymbol{U}_\beta, \quad \tilde{\boldsymbol{M}}_{\alpha\beta}(\{\boldsymbol{X}\}) = \boldsymbol{M}_{\alpha\beta}(\{\boldsymbol{X}\}) + m_\alpha\boldsymbol{I}_{\alpha\beta}, \tag{2.9a,b}$$

where $\boldsymbol{I}_{\alpha\beta}$ is the identity tensor.

The equations of motion for particles in potential flow follow from Lagrangian mechanics, where the Lagrangian is the difference between the kinetic and potential energies $\mathcal{L} = \mathcal{T} - \mathcal{V}$. For particle α

$$\frac{\mathrm{d}}{\mathrm{d}t}\frac{\partial\mathcal{L}}{\partial\boldsymbol{U}_\alpha} - \frac{\partial\mathcal{L}}{\partial\boldsymbol{x}_\alpha} = \boldsymbol{F}_\alpha^C, \tag{2.10}$$

where we have not assumed that the connector forces are derivable from a potential (although they may be). We have assumed that the flow field is inviscid, such that viscous forces are negligible, but this assumption can be relaxed (see § 4). The kinetic energy term on the left-hand side of (2.10) can be shown to give the net pressure force integrated over the body (Lamb 1924). From the Lagrangian, the generalized momentum of particle α is

$$\boldsymbol{P}_\alpha = \sum_{\beta=1}^{N}\tilde{\boldsymbol{M}}_{\alpha\beta}\cdot\boldsymbol{U}_\beta, \tag{2.11}$$

and $\mathrm{d}\boldsymbol{P}_\alpha/\mathrm{d}t$ gives the left-hand side of (2.10) (without the potential $\mathcal{V}$). The generalized momentum accounts for both the intrinsic momentum of the particle and the added momentum resulting from the motion of the fluid.

The total momentum of the body (and fluid) composed of N particles is the sum over the individual generalized momenta: $\boldsymbol{P}_{body} = \sum_\alpha \boldsymbol{P}_\alpha$, and since the internal connector forces sum to zero, we have $\mathrm{d}\boldsymbol{P}_{body}/\mathrm{d}t = 0$ or

$$\boldsymbol{P}_{body} = \sum_{\alpha,\beta=1}^{N}\tilde{\boldsymbol{M}}_{\alpha\beta}\cdot\boldsymbol{U}_\beta = \boldsymbol{C}, \tag{2.12}$$

where $\boldsymbol{C}$ is a constant vector. Our interest is in motion due to the deformation of the body, and therefore we set any constant momentum to zero. From (2.12) it is easy to see that if we define the relative coordinates and velocities as in (2.3*a*,*b*) then the net displacement

in one period is identical to (2.6) for Stokes flow with the resistance tensor replaced by the added mass matrix:

$$\Delta \boldsymbol{x}_1 = -\int_0^T \tilde{\boldsymbol{M}}_{body}^{-1}(t) \cdot \sum_{\alpha,\beta=1}^{N} \tilde{\boldsymbol{M}}_{\alpha\beta}(t) \cdot \boldsymbol{V}_\beta(t)\, \mathrm{d}t, \tag{2.13}$$

where, as before, the body's added mass is $\tilde{\boldsymbol{M}}_{body} = \sum_{\alpha,\beta=1}^{N} \tilde{\boldsymbol{M}}_{\alpha\beta}$. The integration by parts (2.7) also follows by simple replacement.

Thus, as first shown by Chambrion *et al.* (2019), we see that self-propulsion in potential flow takes a form identical to that for Stokes flow with the added mass matrix replacing the resistance matrix. This equivalence follows directly from the zero net force balance and the fact that the viscous hydrodynamic force in Stokes flow and the linear momentum in potential flow are linear in the particle velocities. While the structure is the same, this does not mean the net displacement is the same in the two flows, as the magnitude and form of the interactions, and thus the values of the components of resistance and added mass matrices, are different.

The forms of the net motion given above apply for any 'gate' of the swimmer, i.e. any $\boldsymbol{V}_\beta(t)$. The details of how the body articulates its component parts are not needed. A swimmer can have a fixed gate and then the internal forces $\boldsymbol{F}^C$ necessary to achieve that gate can be found from the individual force balances once the locator point motion is known. Alternatively, the activation of the internal forces could be prescribed and then the articulation and net displacement of the body can be found. It is also possible to have more complex dynamics in terms of control functions or swimming with a fixed power consumption. They each follow the above analysis.

3. Collinear swimmer

As an illustration of swimming in potential flow and how it compares with that in Stokes flow, we consider the prototypical Stokes swimmer design analogous to that of Najafi & Golestanian (2004), which distils the hydrodynamic mechanism of self-propulsion into a minimal model. The swimmer consists of three identical spheres connected via two 'arms' (figure 2). The arms are thin, such that we can neglect them hydrodynamically. The body is collinear and its locater point and kinematic constraints are relative to the central particle 2, such that

$$\boldsymbol{r}_1 = \left(\bar{R} + \frac{U_0}{\omega}\sin(\omega t)\right)\boldsymbol{e}_x \quad \text{and} \quad \boldsymbol{r}_3 = -\left(\bar{R} + \frac{U_0}{\omega}\sin(\omega t + \delta)\right)\boldsymbol{e}_x. \tag{3.1a,b}$$

The constrained particles oscillate with amplitude U_0/ω, frequency ω and phase shift δ. The time-averaged moment arm $\bar{R}$ over the articulation period is identical for both oscillators. One may alter the constraints' functional form and the discussion will not change significantly. The key aspects are that the motion is periodic and there is an out-of-phase component between at least two degrees of freedom.

The body is initially collinear along the x-axis, and all articulation occurs along this axis. By symmetry the swimmer will remain along this axis for all time and the spatial degrees of freedom are reduced to one. For potential flow, we have set the particle densities equal to that of the fluid $\rho_p = \rho_f$. To gain further analytical insight into the structure of self-propulsion, we calculate the leading-order Taylor expansion of the body equations of motions in both flow regimes ((2.6) and (2.13)). The expansion accuracy is captured by the small parameter $\varepsilon = (U_0/\omega)/\bar{R}$, which is the ratio of the oscillation amplitude to the

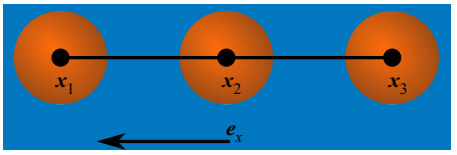

Figure 2. Three spheres of equal radii a are connected by thin arms with prescribed kinematics. The swimmer is collinear and translates along one spatial dimension.

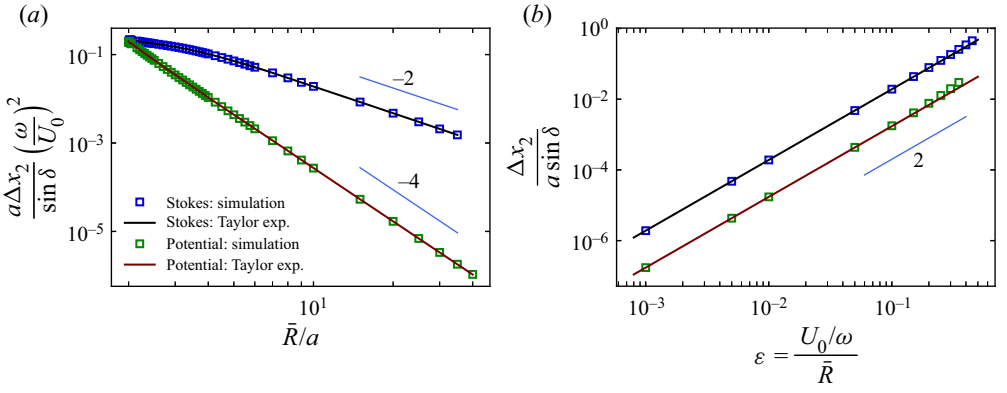

Figure 3. The self-propulsion of the collinear swimmer after one period of articulation. Particles were neutrally buoyant, and simulated with phase angle $\delta = \pi/2$. Self-propulsion is inversely proportional to the average interparticle spacing (a) with $U_0/(a\omega) = 0.01$ and proportional to relative dimensionless oscillation (b).

time-averaged interparticle separation. In this limit, the hydrodynamic interactions during the articulation are well-approximated by their values at the time-averaged separation, and the leading-order results for Stokes and potential flow are

$$\Delta x_2 = 2\pi \sin\delta \left(\frac{U_0}{\omega}\right)^2 \left.\frac{\partial \mathcal{R}_{B3}}{\partial r_3}\right|_{r_1=\bar{R},r_3=-\bar{R}} \quad \text{and}$$

$$\Delta x_2 = 2\,\pi \sin\delta \left(\frac{U_0}{\omega}\right)^2 \left.\frac{\partial \mathcal{M}_{B3}}{\partial r_3}\right|_{r_1=\bar{R},r_3=-\bar{R}}, \tag{3.2a,b}$$

respectively, where the detailed forms of $\mathcal{R}_{B3}$ and $\mathcal{M}_{B3}$ can be found in Appendix B).

The Stokes swimmer translates farther after an articulation period when the particles are well-separated, as seen in figure 3(a). This behaviour arises from the stronger hydrodynamic interactions in Stokes flow at large separations. From (2.7) self-propulsion scales with the gradient of the configuration-dependent hydrodynamic tensors. A translating sphere in Stokes flow creates a monopolar disturbance (Durlofsky, Brady & Bossis 1987), giving a leading-order net translation scaling of $O(\bar{R}^{-2})$. In potential flow, the longest ranged hydrodynamic interaction scales as a dipolar gradient (Yurkovetsky & Brady 1996), which gives an $O(\bar{R}^{-4})$ scaling for net translation. Full numerical simulation of the equations of motion ((2.7) and (2.13)) matches the analytical predictions very well. At narrow separations, the higher-order moments accounted for in Stokesian dynamics dominate and reduce the net translation (Durlofsky *et al.* 1987). Simulations and analysis did not account for the singular Stokes-flow lubrication forces at narrow separation.

When the amplitude of articulation ε grows, the Taylor expansion is less accurate as the particles become closer at minimum separation. The inverse power-law scaling of the hydrodynamic interactions causes the closer interactions to overcompensate for the weaker interactions when the particles are at maximum separation and lead to a nonlinear increase in displacement after one period. This results in a deviation between the analytic and numeric results for large amplitude in figure 3(*b*). Nevertheless, the $O(\varepsilon^2)$ scaling of the amplitude of self-propulsion holds even as the oscillation amplitude becomes large compared with average separation and the particles nearly overlap. Note that $\varepsilon \leq \frac{1}{2}$ to prevent particle overlap.

4. Discussion

Self-propulsion in Stokes and potential flow follow an identical structure where time-reversal symmetry is broken through configuration-dependent hydrodynamics, in accord with prior studies (Saffman 1967; Purcell 1977; Kanso *et al.* 2005; Golestanian & Ajdari 2008; Chambrion *et al.* 2019). In potential flow, the kinetic energy is a quadratic function of the velocities, $\mathcal{T} = \frac{1}{2}\boldsymbol{U} \cdot \boldsymbol{M}(\{\boldsymbol{X}\}) \cdot \boldsymbol{U}$, from which it follows that the generalized momentum $\boldsymbol{P} = \partial\mathcal{T}/\partial\boldsymbol{U}$ is linear in the velocities. Stokes flow can be cast into the same form with the Rayleigh dissipation function replacing the kinetic energy: $\dot{\Phi} = \frac{1}{2}\boldsymbol{U} \cdot \boldsymbol{R}(\{\boldsymbol{X}\}) \cdot \boldsymbol{U}$, and the viscous hydrodynamic forces are given by $\boldsymbol{F}^{vis} = -\partial\dot{\Phi}/\partial\boldsymbol{U}$. The quadratic forms show that the mass and resistance tensors are symmetric and positive definite.

It is also possible to combine the two approaches and add the viscous forces to the right-hand side of (2.10) to allow a continuous transition as the Reynolds number increases between self-propulsion in Stokes flow to that in potential flow. Such an approach neglects the nonlinear convection of vorticity, of course, but it may provide a simple way to model the transition between the two regimes. In fact, potential flow can itself generate viscous forces which can be found from the point-wise energy dissipation $\dot{\Phi} = \mu \int \boldsymbol{e} : \boldsymbol{e}\,\mathrm{d}V = \mu \int |\nabla\nabla\phi|^2\,\mathrm{d}V$, where $\boldsymbol{e}$ is the velocity gradient tensor and the integration is over the fluid volume. A translating sphere in potential flow experiences a viscous drag force of $\boldsymbol{F}^{vis} = -12\pi\mu a\boldsymbol{U}$, which is twice that in Stokes flow. It would be interesting to see what insight this combined approach can give to self-propulsion at finite Reynolds numbers.

Despite the geometric similarity, it is still surprising that self-propulsion is possible in potential flow where the motion is fully conservative and the deforming body does no net work on the fluid after each period of articulation. At the end of one period the body shape and the kinetic (and potential) energies return to their original values, but the body has achieved a net displacement. Furthermore, when the body stops deforming, all motion in the fluid ceases instantaneously – there is no time in Laplace's equation – just as it does in Stokes flow.

The three-sphere collinear swimmer was chosen to illustrate the essential features of self-propulsion and shows that the potential swimmer is 'slower' due to the stronger hydrodynamic interactions in Stokes flow. A perhaps even simpler system is to have just two spherical particles, but now allow the radius of one (or both) particles to grow and shrink in time. The separation between the two spheres can be varied in such a way so that the hydrodynamics on inflation differs from that upon deflation which will lead to net motion, as shown by Avron, Kenneth & Oaknin (2005). In this case, both the Stokes and potential-flow disturbances decay as one over separation, and it is not obvious which swimmer is faster, or if this type of deformation can lead to faster translation in general.

We modelled the self-propelling body as a collection of spherical particles, but this was done for simplicity. The individual particles can be of any size, shape and distribution. In the limit where the articulating particles are all small and located along the surface of the body we can achieve a body with surface activation, which is called a squirmer in the Stokes regime. Squirmers have proved to be a simple model and a work horse for the study of active matter systems at low Reynolds number (Lighthill 1952; Swan *et al.* 2011; Theers *et al.* 2018; Datt & Elfring 2019). Indeed, the so-called 'neutral' Stokes squirmer, like a classical phoretic particle, generates a potential-dipole flow field (it has no stresslet); although technically the fluid satisfies the no-slip condition at the particle surface rather than the no-flux condition of potential flow, but that may be just a detail in relating the strength of the potential flow to the nature of the body deformation.

We discussed a single articulating body in this work, but it should be clear from the general formulation that there is no restriction on the number of self-propelled bodies. The study of many interacting self-propelled bodies has become a very vibrant area of research in the active matter community (Pooley, Alexander & Yeomans 2007; Lauga & Bartolo 2008; Cates & Tailleur 2015; Dulaney & Brady 2021; Mallory, Omar & Brady 2021). Active Stokes flow swimmers form the basis of the active Brownian particle (ABP) model for active matter, which has been shown to display very interesting collective dynamics such as motility-induced phase separation (MIPS) and coherent flocking motion. It would be interesting to see if potential swimmers can also display similar collective motion. Two bodies translating parallel to each other may attract due to the Bernoulli effect – to conserve mass the fluid velocity between the two bodies is faster than on the outside – leading to a reduced pressure there and an attractive force. Two bodies moving towards each other along their line of centres will experience a repulsive force as there is a stagnation point between the two bodies and a larger pressure. This simple observation may point to a fluid mechanical origin for flocking structure.

Modelling the fluid motion as potential flow is, of course, a very bold approximation, but it may help give insight into behaviour in situations in which the vorticity is confined to thin regions. This occurs for small amplitude oscillations (see squirmers above) where the vorticity is confined to the body surface, and for streamlined bodies where the vorticity is confined to a thin wake. Outside these thin regions of vorticity the fluid motion at high Reynolds numbers can be modelled as inviscid potential flow (Saffman 1992). If two bodies are swimming side-by-side, when one body changes its speed or direction, the second body will sense this change via the potential-flow interactions before vorticity has time to evolve. Thus, potential flow might prove to be a fruitful starting point.

As a final note, since potential flow is conservative, the system has a Hamiltonian and therefore can have well-defined statistical mechanics and thermodynamics. This was shown to be the case for bubbly liquids by Yurkovetsky & Brady (1996), and used to predict an actual phase transition in a bubbly flow. The study of swimmers in potential flow has a well-founded and developed mechanics and may offer insight into the beautiful and striking collective behaviour often observed in the natural world.

Funding. This work was supported in part by grant CBET 1803662 from the National Science Foundation.

Declaration of interests. The authors report no conflict of interest.

Author ORCIDs.
Alec Glisman https://orcid.org/0000-0001-9677-1958;
John F. Brady https://orcid.org/0000-0001-5817-9128.

Appendix A. Force & torque balance

Here we extend the treatment to include rotary motion of the particles and the body along with the associated torque and angular momentum balances. We group the force ($\boldsymbol{F}$) and torque ($\boldsymbol{L}$) on particle α into a single vector $\mathcal{F}_\alpha = (\boldsymbol{F}_\alpha, \boldsymbol{L}_\alpha)$, and likewise for the translational and rotational velocities $\mathcal{U}_\alpha = (\boldsymbol{U}_\alpha, \boldsymbol{\Omega}_\alpha)$, where the angular velocity $\boldsymbol{\Omega}_\alpha$ is about the centre of particle α. In Stokes flow, the viscous hydrodynamic drag force/torque on particle α is

$$\mathcal{F}_\alpha^{vis} = -\mathcal{R}_{\alpha\beta} \cdot \mathcal{U}_\beta, \tag{A1}$$

with an implied sum over all particles β and the 'grand' resistance matrix $\mathcal{R}_{\alpha\beta}$ is a function of the positions and orientations of all N particles.

Denoting the translational and rotational velocity of the body by $\mathcal{U}_B = (\boldsymbol{U}_B, \boldsymbol{\Omega}_B)$, and following Swan *et al.* (2011) we define the relative velocities $\mathcal{V}_\beta$ of each particle by

$$\mathcal{U}_\beta = \boldsymbol{\Sigma}^T \cdot \mathcal{U}_B + \mathcal{V}_\beta, \tag{A2}$$

where the tensor $\boldsymbol{\Sigma}$ is composed of 6×6 submatrices connecting the body locator point B to each particle of the form

$$\boldsymbol{\Sigma}_{B\alpha} = \begin{pmatrix} 1 & 0 & 0 & 0 & 0 & 0 \\ 0 & 1 & 0 & 0 & 0 & 0 \\ 0 & 0 & 1 & 0 & 0 & 0 \\ 0 & \Delta r_3^{\alpha B} & -\Delta r_2^{\alpha B} & 1 & 0 & 0 \\ -\Delta r_3^{\alpha B} & 0 & \Delta r_1^{\alpha B} & 0 & 1 & 0 \\ \Delta r_2^{\alpha B} & -\Delta r_1^{\alpha B} & 0 & 0 & 0 & 1 \end{pmatrix}, \tag{A3}$$

where $\Delta \boldsymbol{r}^{\alpha B} = \boldsymbol{x}_\alpha - \boldsymbol{x}_B$. These submatrices connecting each of the N particles to the locator point are assembled into the rigid body connectivity matrix $\boldsymbol{\Sigma}$.

The connectivity matrix $\boldsymbol{\Sigma}$ sums the forces and torques on all the particles, and since the net internal forces and torques are zero, $\boldsymbol{\Sigma} \cdot \mathcal{F}^C = 0$, summing (A1) along with the relative velocities (A2) gives the motion of the body in Stokes flow:

$$\mathcal{U}_B^{Stokes} = -\left(\boldsymbol{\Sigma} \cdot \mathcal{R} \cdot \boldsymbol{\Sigma}^T\right)^{-1} \cdot \boldsymbol{\Sigma} \cdot \mathcal{R} \cdot \mathcal{V}, \tag{A4}$$

where we have suppressed the subscripts and the implied sum is over all particles. Equation (A4) is the generalization of (2.5) to include the torque balance. The form is the same and therefore the net displacement over a period follows by integration in time.

In potential flow the total kinetic energy of the N-particle system including the angular velocities has the quadratic form $\mathcal{T} = \frac{1}{2}\sum_{\alpha\beta} \mathcal{U}_\alpha \cdot \tilde{\mathcal{M}}_{\alpha\beta} \cdot \mathcal{U}_\beta$, where the added mass matrix now also contains the individual particles' moments of inertia. The generalized momentum (linear and angular) of particle α is $\mathcal{P}_\alpha = \sum_\beta \tilde{\mathcal{M}}_{\alpha\beta} \cdot \mathcal{U}_\beta$. The total linear and angular momentum is a constant, which we take to be zero, and using $\boldsymbol{\Sigma}$ and the relative velocities we have (A4), but with the added mass matrix replacing the grand resistance matrix for potential flow:

$$\mathcal{U}_B^{Potential} = -\left(\boldsymbol{\Sigma} \cdot \tilde{\mathcal{M}} \cdot \boldsymbol{\Sigma}^T\right)^{-1} \cdot \boldsymbol{\Sigma} \cdot \tilde{\mathcal{M}} \cdot \mathcal{V}; \tag{A5}$$

integration over a period, gives the analogue of (2.13).

Appendix B. $\mathcal{R}_{B3}$ and $\mathcal{M}_{B3}$

The subscript B reflects that the quantities contain information about the body's overall configuration. The effective resistance tensor is given as $\mathcal{R}_{B3} = R_{body}^{-1} \sum_{\alpha=1}^{3} R_{\alpha 3}$, while the effective mass tensor $\mathcal{M}_{B3}$ is identical in form with R replaced by $\tilde{\mathcal{M}}$. Detailed calculation of specific tensor elements can be found in Durlofsky *et al.* (1987) for Stokes flow and Yurkovetsky & Brady (1996) for potential flow. The leading-order effective mass matrix is given as

$$\mathcal{M}_{B3} = \frac{3 - 2\left(\dfrac{1}{r_{23}^3} - \dfrac{1}{r_{13}^3}\right)}{9 - 4\left(\dfrac{1}{r_{13}^3} - \dfrac{1}{r_{23}^3} - \dfrac{1}{r_{12}^3}\right)}, \tag{B1}$$

where r_{ij} is the distance between particles i and j. The effective resistance matrix was evaluated numerically using Stokesian dynamics without lubrication forces.

References

Avron, J.E., Kenneth, O. & Oaknin, D.H. 2005 Pushmepullyou: an efficient micro-swimmer. *New J. Phys.* **7** (1), 234.

Cates, M.E. & Tailleur, J. 2015 Motility-induced phase separation. *Annu. Rev. Condens. Matter Phys.* **6** (1), 219–244.

Chambrion, T., Giraldi, L. & Munnier, A. 2019 Optimal strokes for driftless swimmers: a general geometric approach. *ESAIM: Control Optim. Calculus Variations* **25**, 6.

Datt, C. & Elfring, G.J. 2019 Active particles in viscosity gradients. *Phys. Rev. Lett.* **123** (15), 158006.

Dulaney, A.R. & Brady, J.F. 2021 Machine learning for phase behavior in active matter systems. *Soft Matt.* **17** (28), 6808–6816.

Durlofsky, L., Brady, J.F. & Bossis, G. 1987 Dynamic simulation of hydrodynamically interacting particles. *J. Fluid Mech.* **180**, 21–49.

Golestanian, R. & Ajdari, A. 2008 Analytic results for the three-sphere swimmer at low Reynolds number. *Phys. Rev.* E **77** (3), 036308.

Kanso, E., Marsden, J.E., Rowley, C.W. & Melli-Huber, J.B. 2005 Locomotion of articulated bodies in a perfect fluid. *J. Nonlinear Sci.* **15** (4), 255–289.

Klotsa, D. 2019 As above, so below, and also in between: mesoscale active matter in fluids. *Soft Matt.* **15** (44), 8946–8950.

Lamb, H. 1924 *Hydrodynamics*. University Press.

Lauga, E. & Bartolo, D. 2008 No many-scallop theorem: collective locomotion of reciprocal swimmers. *Phys. Rev.* E **78** (3), 030901.

Lauga, E. & Powers, T.R. 2009 The hydrodynamics of swimming microorganisms. *Rep. Prog. Phys.* **72** (9), 096601.

Lighthill, M.J. 1952 On the squirming motion of nearly spherical deformable bodies through liquids at very small Reynolds numbers. *Commun. Pure Appl. Maths* **5** (2), 109–118.

Lighthill, S.J. 1975 *Mathematical Biofluiddynamics*. SIAM.

Mallory, S.A., Omar, A.K. & Brady, J.F. 2021 Dynamic overlap concentration scale of active colloids. *Phys. Rev.* E **104** (4), 044612.

Masoud, H. & Stone, H.A. 2019 The reciprocal theorem in fluid dynamics and transport phenomena. *J. Fluid Mech.* **879**, P1.

Najafi, A. & Golestanian, R. 2004 Simple swimmer at low Reynolds number: three linked spheres. *Phys. Rev.* E **69** (6), 062901.

Pooley, C.M., Alexander, G.P. & Yeomans, J.M. 2007 Hydrodynamic interaction between two swimmers at low Reynolds number. *Phys. Rev. Lett.* **99** (22), 228103.

Purcell, E.M. 1977 Life at low Reynolds number. *Am. J. Phys.* **45** (1), 3–11.

Saffman, P.G. 1967 The self-propulsion of a deformable body in a perfect fluid. *J. Fluid Mech.* **28** (2), 385–389.

Saffman, P.G. 1992 *Vortex Dynamics*. Cambridge University Press.

STONE, H.A. & SAMUEL, A.D.T. 1996 Propulsion of microorganisms by surface distortions. *Phys. Rev. Lett.* **77** (19), 4102.

SWAN, J.W., BRADY, J.F., MOORE, R.S. & CHE 174 2011 Modeling hydrodynamic self-propulsion with Stokesian dynamics. Or teaching Stokesian dynamics to swim. *Phys. Fluids* **23** (7), 071901.

THEERS, M., WESTPHAL, E., QI, K., WINKLER, R.G. & GOMPPER, G. 2018 Clustering of microswimmers: interplay of shape and hydrodynamics. *Soft Matt.* **14** (42), 8590–8603.

WU, T. 1971 Hydromechanics of swimming propulsion. Part 1. Swimming of a two-dimensional flexible plate at variable forward speeds in an inviscid fluid. *J. Fluid Mech.* **46** (2), 337–355.

WU, T., BROKAW, C.J. & BRENNEN, C. 1975 *Swimming and Flying in Nature*. Springer.

YURKOVETSKY, Y. & BRADY, J.F. 1996 Statistical mechanics of bubbly liquids. *Phys. Fluids* **8** (4), 881–895.